Broadband microcomb generation in silica spherical microresonators with engineered dispersive waves in normal and anomalous dispersion regime

YOU GAO[1], SUWAN SUN[1], XUKUN LIN[1], KAILIN WU[1], XIAOYING WANG[1], HAIYUN YUAN[1], JIAMIN BAI[1], SIYU WANG[1], AND HAIRUN GUO[1,*]

[1]Key Laboratory of Specialty Fiber Optics and Optical Access Networks, Joint International Research Laboratory of Specialty Fiber Optics and Advanced Communication, Shanghai University, Shanghai 200444, China
[*]hairun.guo@shu.edu.cn

Compiled August 25, 2023

Expanding the bandwidth of frequency combs in microcavities is currently a prominent research area, and one effective approach is to introduce dispersive waves using higher-order dispersion. However, The exploration of high-order dispersion control on quartz microsphere platforms has been limited by the challenge of preserving high Q factors across a broad range of sizes. Here, we fabricated quartz microspheres through arc discharge with diameters ranging from 100-260 μm, achieving Q factors in the range of 10^8. We achieved a broadband Kerr frequency comb with dispersive wave radiation by manipulating the dispersion of the microsphere through size adjustment. Our experimental results demonstrate that the spectral span of the dispersive wave frequency combs can extend up to 360 nm. At the same time, we have also demonstrated Raman lasers and Raman-Kerr frequency combs in small microspheres with normal dispersion.This work provides a reference for developing broadband, high-coherence frequency combs on microsphere platforms and offers an efficient implementation scheme for low-noise integrated broadband frequency combs.

http://dx.doi.org/10.1364/ao.XX.XXXXXX

The potential of optical frequency comb (OFC) has been demonstrated in various applications, such as massive parallel optical communications [1, 2], optical data centers [3, 4] , massive parallel LIDAR [5], low-noise microwave synthesis [6, 7], and photonic neural computing [8, 9] .

In recent years, the optical frequency combs technology based on high Q microcavities has received widespread attention from both domestic and international researchers [10–13]. Currently, fully integrated and highly compact optical frequency combs chips have been realized, providing a multitude of high-performance laser sources for advanced optical metrology [14–18]. In addition, microcavity frequency combs have been shown to have tremendous application prospects in areas such as massive parallel optical communications [1, 2], optical data centers [3, 4], massive parallel LIDAR [5], low-noise microwave synthesis [6, 7], and photonic neural computing [8, 9]. The WGM microcavity is a significant platform for investigating microcavity frequency comb technology and served as one of the pioneering platforms in this field of research. In particular, the WGM microcavities, such as crystalline fluoride resonators, have achieved ultra-high Q factors up to 10^{11} and finesse up to 10^7 [19]. Many classic theories and experimental phenomena of microcavity frequency combs have been verified in WGM microcavities, including the formation of dissipative temporal solitons [2, 10, 20–22], soliton pulse scaling [23], soliton number switching [24, 25], soliton breathers [26], and soliton behaviors to intermode interactions [27].

Usually, Research on broadening frequency combs in WGM microcavities is essential for applications requiring broad spectral coherence, such as spectroscopy, precision frequency metrology, and optical clocks. Introducing dispersion waves (DWs) through higher-order dispersion is an effective way to extend the spectrum. Previous studies have extensively investigated the processes of mode locking, soliton formation, and DWs generation in optical microcavities based on silicon nitride (Si_3N_4) and aluminum nitride (AlN) platforms [12, 28–31], as well as the role of higher-order dispersion [32–34], which is of significant importance in verifying the dispersion engineering required for generating broadband Kerr frequency combs [35]. It is established that microcavity dispersion can be manipulated via microcavity size control to convert anomalous dispersion to normal dispersion [36]. However, there is relatively little work on dispersion management in quartz microspheres, and the current main method for generating DWs frequency combs in quartz microspheres is by adding coatings to the surface of the microspheres.

In this paper, we have studied the dispersion characteristics of them with different sizes by preparing the microsphere resonators and have successfully generated broadband DWs frequency combs [37]. Meanwhile, we have also demonstrated Raman lasers and Raman-Kerr frequency combs in a 130 μm diameter microsphere with normal dispersion. This work provides a valuable reference for the development of broadband

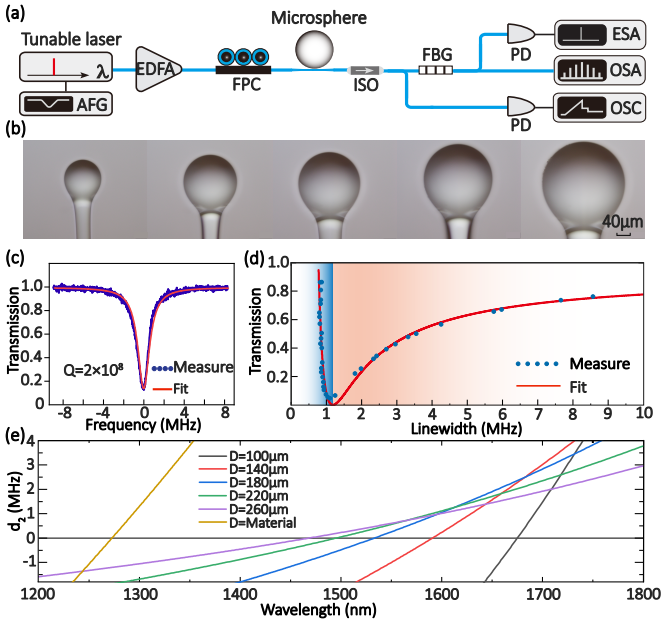

Fig. 1. Preparation and characterization of microsphere resonator. (a) A schematic of the experimental setup. AFG: arbitrary function generator, EDFA: Erbium-doped fiber amplifier, OSC: oscilloscope, ESA: electrical spectrum analyzer, OSA: Optical spectrum analyzer. (b) Preparation of microsphere resonators with diameters of 100 μm, 180 μm, 200 μm, 220 μm and 260 μm. (c) The measured transmitted power trace of one resonance of a 200 μm diameter microsphere resonator,and fitting with Lorentz linear function. (d) Assessment of the ideality of the resonant modes in the microsphere resonator. (e) Dispersion coefficient d_2 of microsphere resonators with different sizes.

and highly coherent frequency combs in quartz microspheres.

First, we used the arc discharge method, in which high-voltage discharges were generated at the position of the fiber end face using a fusion splicer, and a short-pulsed arc rapidly melted it. Under the effect of surface tension, a quartz microsphere resonator was formed at the fiber end face. So we prepared microsphere resonators with diameters ranging from 100-260 μm, as shown in Fig. 1(b). We then utilized the experimental system (Fig. 1(a)) to measure the transmission of a 200 μm diameter microsphere resonance by scanning the cw diode laser over it. Using Lorentz linear fitting, the results showed that the Q value in the microcavity was approximately 2×10^8, and it was determined that the FSR is 330.52 GHz. as shown in Fig. 1(c). In addition, the coupling ideality with respect to selected resonant mode of the resonator is characterized, see 1(d), which is on a high-level indicating almost no loss at the coupling junction.

Meanwhile, we used the same experimental method to test microsphere resonators, and the linewidth and intrinsic Q values are shown in Table 1.

Another important parameter of microsphere resonator is dispersion, which affects the coherence of the comb spectrum and the generation of spectral bandwidth. The formation of DWs caused by higher-order dispersion terms may result in the comb spectrum to enter into the normal dispersion state. The total dispersion of the optical microcavity is determined by both material dispersion and geometric dispersion, and the dispersion size can be controlled by adjusting the material and structure to

Table 1. Q value of microsphere cavities with different sizes.

Diameter (μm)	Linewidth (MHz)	Q_0
100	2.30	0.84×10^8
180	1.19	1.62×10^8
200	0.95	2.00×10^8
220	1.86	1.00×10^8
260	1.40	1.38×10^8

achieve an ideal dispersion distribution for the microcavity. The geometric dispersion of microsphere can be directly controlled by their size. Here, the DWs of microsphere resonators with diameters of 100 μm,140 μm,180 μm, 220 μm and 260 μm are simulated, see Fig. 1(e).

As indicated by the simulation results, a diameter of 140 μm microsphere resonator exhibits normal dispersion near the 1550 nm pump, with a zero dispersion point located close to the pump position, offering the opportunity to cross into the anomalous dispersion region and generate Kerr frequency combs. In contrast, a diameter of 100 μm microsphere remains in the normal dispersion regime even at a distance from the 1550 nm pump, making it difficult to generate Kerr frequency combs. The position of the zero dispersion point (d_2=0) shifts towards shorter wavelengths as the diameter of the microsphere resonator increases. Before 1580 nm, the value of d_2 increases as the diameter of microsphere increases, resulting in a less flat d_{int} and an increasing anomalous dispersion region. Conversely, when the diameter of microsphere decreases, the dispersion gradually enters the normal dispersion region.

By changing the dispersion curve, it can be seen that changing the diameter of the microsphere from 100 μm to 260 μm gradually shifts the position of the dispersion waves to shorter wavelengths. This demonstrates that the size variation of the microsphere can lead to effective dispersion control.

We utilized the experimental setup to realize frequency combs of DWs, Raman laser, and Kerr frequency combs, as well as Raman-Kerr frequency combs, in microspheres with diameters of 160 μm, 180 μm, and 200 μm, see Fig.1(b). We simulated the integrated dispersion curves (d_{int}) generated for the three different-sized microspheres, while also predicting the positions of the DWs(the intersection points with d_{int}=0), see Fig.2(a). As the diameter of the microspheres increased, significant changes were observed in the microsphere dispersion, with the dispersion curves continually increasing in height and the positions of the DWs gradually moving towards shorter wavelengths. We next carried out experiments for DWs frequency combs generation in a 200 μm diameter microsphere resonators. When the input power was approximately 280 mW and tuning the laser from the blue-detuned side, we observed the evolution of the spectrum through the primary combs, modulation instability (MI) combs, and DWs frequency combs via tuning, see Fig. 2(b,c,d). Although the spectral envelope appeared smooth, there were still breaches, which may have been caused by the lack of optimal matching with the modal dispersion or the influence of other modes.

In addition, we use the same experimental method to generate broadband DWs frequency combs in 160 μm and 180 μm diameter microsphere resonators. Furthermore, by comparing the simulation and experimental results of three different sizes of microsphere resonators, we found that the dispersion wave

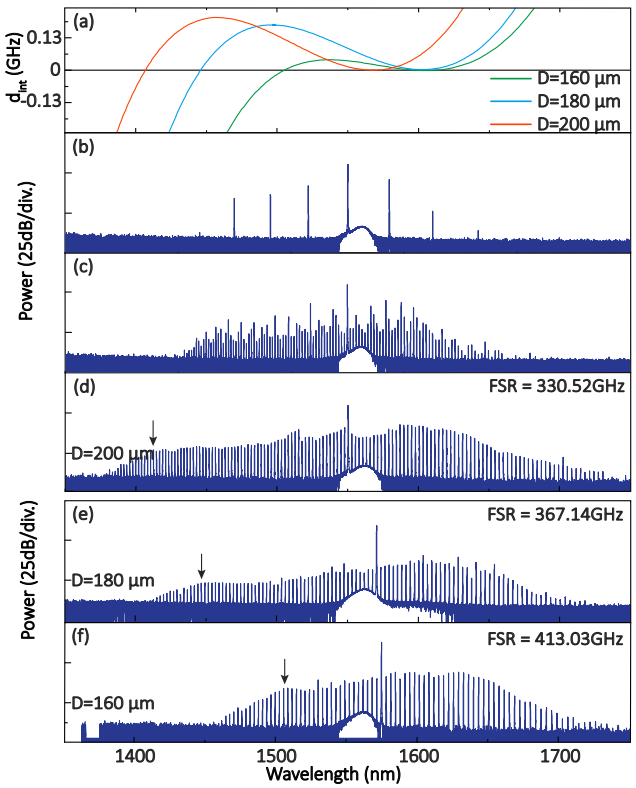

Fig. 2. The d_{int} curve and DWs frequency combs spectrum of microsphere with diameter of 160 μm, 180 μm and 200 μm. (a) d_{int} curve of microsphere resonator with diameter of 160 μm, 180 μm and 200 μm. (b,c) DWs frequency combs spectra of microsphere cavities with diameters of 160 μm (Pump power is 207 mW) and 180 μm (Pump power is 224 mW). (d,e,f) The evolution process of the microsphere with a diameter of 200 μm from the primary comb, MI, and DWs frequency combs (the pump power is 280 mW).

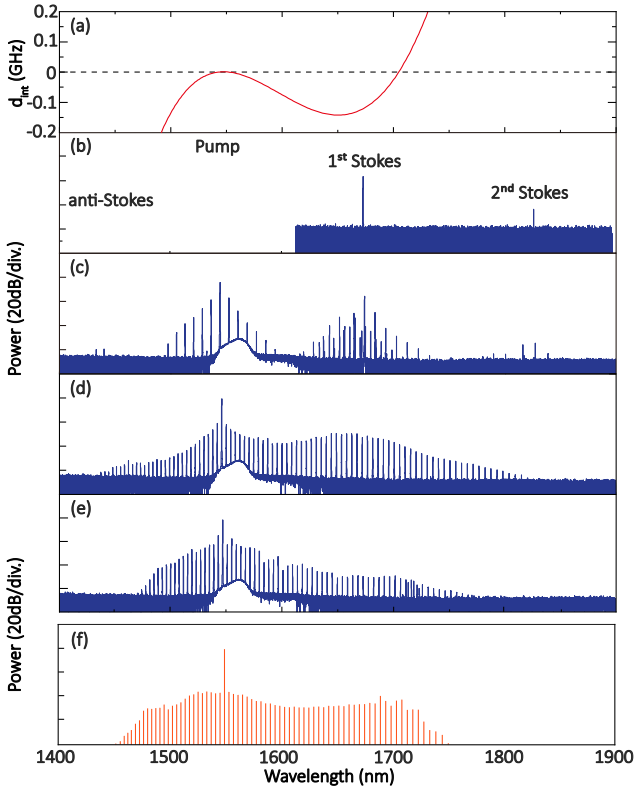

Fig. 3. Raman laser, Raman-Kerr frequency combs and DWs frequency combs of 130 μm diameter microsphere resonator. (a) The d_{int} curve of microsphere resonator at 1547.73 nm. (b) pump is Raman laser generated at 1542.7 nm. (c) The Raman Kerr frequency combs with local different mode families are generated at 1543.9 nm. (d) The pump is 1546.9 nm, which produces a Raman Kerr frequency comb with Kerr effect enhancement. (e) DWs frequency combs generation. (f) Simulation of DWs frequency combs when the pump is 1547.73 nm (d_2=13.5 MHz, d_3=1.5 MHz).

position of the experiment is in good agreement with the simulation. Meanwhile,The spectral spans exceeded 280 nm for all microspheres, with a maximum spectral span of 360 nm.

Finally, we generate a broadband frequency combs with normal dispersion in a 130 μm diameter microsphere resonator. Fig. 3 illustrates the process of Raman laser, Raman-Kerr frequency combs, and DWs frequency combs generated during the long-wavelength tuning of the pumping light in a 130 μm diameter microsphere. We calculated the dispersion distribution d_{int} of 130 μm microsphere, and we can see that the microsphere at this size is in the normal dispersion region, as shown in Fig. 3(a), When the pumping was tuned to 1542.7 nm, a Raman laser was generated, and a clearly visible first-order Stokes laser with a frequency shift of approximately 3.755 THz, close to the center peak of Raman gain, was observed at 1672 nm. Furthermore, a second-order Stokes laser could be observed at 1826 nm, and a weaker anti-Stokes laser could be observed at 1431.6 nm on the short-wavelength side of the pumping light,see Fig. 3(b).

This phenomenon is due to the overlap of the resonant peak of microsphere with the wide Raman gain, resulting in a Raman laser dominated by Raman oscillation. From Fig. 3(c), it can be observed that when the pump is tuned to 1543.9 nm, numerous sidebands are generated around both the Raman laser and the pump laser. This is due to the large energy accumulation in microsphere resonator, which transfers the energy to adjacent resonant modes that happen to be located within the MI gain band, thus exciting the Kerr frequency combs. at this point, the local Raman-Kerr frequency combs appear on the spectrum, and the dominance of the Raman effect can be inferred from the intensity of the Raman laser. When the pump is tuned to 1546.9 nm, Fig. 3(d) shows an overall increase in spectral intensity with a smoother spectral envelope, and the maximum spectral span is approximately 400 nm. Equally spaced comb teeth indicate that the frequency combs generated near the Raman laser is within the same mode family as the pump mode. However, the intensities at the first-order Stokes and anti-Stokes laser frequencies did not increase, possibly due to the MI gain band being much smaller than the Raman gain band, and the pump detuning being relatively small, making it easy for the resonant peak to approach the peak of the MI gain band. The Raman gain band is relatively wide, and the resonant peak within the gain band is not significantly affected by Raman gain reduction.

Fig. 3(e) indicates that by fine-tuning the coupling position between the tapered fiber and the microsphere based on this experiment, a broadband Kerr frequency combs with almost disappeared Raman effect can be observed in the spectrum, and a small wavelet packet exists at 1702 nm. As it appears at the mid-

point between the first-order Stokes laser and the second-order Stokes laser, it can be inferred that this may be a long-wavelength DWs dominated by the Kerr effect. Moreover, it can be inferred from the d_{int} curve (Fig. 3(a)) and Raman-Kerr frequency combs simulation (Fig. 3(f)) that the wavelength corresponding to d_{int}=0 is very close to the experimental DWs wavelength of 1702 nm, thereby confirming it as a long-wavelength DWs frequency combs.

Therefore, a successful transition from Raman laser to Raman-Kerr frequency combs dominated by Kerr effect was achieved in a microsphere with a diameter of 130 μm. The final result was the conversion to a long-wavelength DWs frequency combs, which verified the competition process between Raman effect and Kerr effect.

In conclusion, we have demonstrated the generation of both DWs frequency combs and Raman-Kerr frequency combs in high-Q microsphere resonators. Microsphere resonators of varying sizes were fabricated using arc discharge, achieving Q values of up to 10^8. Furthermore, dispersion management was achieved by controlling the size of microsphere, and frequency combs with broad bandwidth near the pump wavelength were demonstrated in microspheres of three different sizes. The relationship between the position of the DWs and microsphere cavity diameter was verified. Additionally, the effect of size on the Raman-Kerr competition was observed, with smaller microsphere cavities exhibiting stronger Raman effects and a greater tendency to produce Raman lasers, cascaded Raman effects, and Raman-Kerr frequency combs in the normal dispersion region. As the diameter increased, the Raman effect weakened, making it easier to produce broadband Kerr frequency combs. Furthermore, dispersion can be fine-tuned by adjusting the coupling position between the tapered fiber and microsphere, allowing for the switching between Raman lasers and Kerr frequency combs. This work provides valuable insights for the development of broadband, highly coherent frequency combs in microsphere, laying a foundation for the integration of Kerr frequency combs in this cavities.

Funding. National Key Research and Development Program of China (2020YFA0309400); National Natural Science Foundation of China (11974234); Shanghai Science and Technology Development Foundation (20QA1403500).

Acknowledgments. We acknowledge funding from National Key Research and Development Project of China, National Natural Science Foundation of China, and Shanghai Science and Technology Development Funds. This work is also supported by 111 Project (D20031) by MoE of China. Preforms of the crystalline resonators are fabricated in the Engineering Technology Training Center at Shanghai University.

Disclosures. The authors declare no conflicts of interest.

Data Availability Statement. Data and simulation codes related to this work are available from the corresponding author upon reasonable request.

REFERENCES

1. P. Marin-Palomo, J. N. Kemal, M. Karpov, A. Kordts, J. Pfeifle, M. H. P. Pfeiffer, P. Trocha, S. Wolf, V. Brasch, M. H. Anderson, R. Rosenberger, K. Vijayan, W. Freude, T. J. Kippenberg, and C. Koos, Nature **546**, 274 (2017).
2. S. Fujii, S. Tanaka, T. Ohtsuka, S. Kogure, K. Wada, H. Kumazaki, S. Tasaka, Y. Hashimoto, Y. Kobayashi, T. Araki, K. Furusawa, N. Sekine, S. Kawanishi, and T. Tanabe, Opt. Express **30**, 1351 (2022).
3. A. S. Raja, S. Lange, M. Karpov, K. Shi, X. Fu, R. Behrendt, D. Cletheroe, A. Lukashchuk, I. Haller, F. Karinou, B. Thomsen, K. Jozwik, J. Liu, P. Costa, T. J. Kippenberg, and H. Ballani, Nat. Commun. **12**, 5867 (2021).
4. B. Corcoran, M. Tan, X. Xu, A. Boes, J. Wu, T. G. Nguyen, S. T. Chu, B. E. Little, R. Morandotti, A. Mitchell, and D. J. Moss, Nat. Commun. **11**, 2568 (2020).
5. J. Riemensberger, A. Lukashchuk, M. Karpov, W. Weng, E. Lucas, J. Liu, and T. J. Kippenberg, Nature **581**, 164 (2020).
6. E. Lucas, P. Brochard, R. Bouchand, S. Schilt, T. Südmeyer, and T. J. Kippenberg, Nat. Commun. **11**, 374 (2020).
7. J. Liu, E. Lucas, A. S. Raja, J. He, J. Riemensberger, R. N. Wang, M. Karpov, H. Guo, R. Bouchand, and T. J. Kippenberg, Nat. Photonics **14**, 486 (2020).
8. X. Xu, M. Tan, B. Corcoran, J. Wu, A. Boes, T. G. Nguyen, S. T. Chu, B. E. Little, D. G. Hicks, R. Morandotti, A. Mitchell, and D. J. Moss, Nature **589**, 44 (2021).
9. J. Feldmann, N. Youngblood, M. Karpov, H. Gehring, X. Li, M. Stappers, M. Le Gallo, X. Fu, A. Lukashchuk, A. S. Raja, J. Liu, C. D. Wright, A. Sebastian, T. J. Kippenberg, W. H. P. Pernice, and H. Bhaskaran, Nature **589**, 52 (2021).
10. T. Herr, V. Brasch, J. D. Jost, C. Y. Wang, N. M. Kondratiev, M. L. Gorodetsky, and T. J. Kippenberg, Nat. Photonics **8**, 145 (2014).
11. T. Liu, S. Sun, Y. Gao, S. Wang, Y. Chu, and H. Guo, Photonics Res. **10**, 2866 (2022).
12. V. Brasch, M. Geiselmann, T. Herr, G. Lihachev, M. H. P. Pfeiffer, M. L. Gorodetsky, and T. J. Kippenberg, Science **351**, 357 (2016).
13. T. J. Kippenberg, A. L. Gaeta, M. Lipson, and M. L. Gorodetsky, Science **361**, eaan8083 (2018).
14. B. Stern, X. Ji, Y. Okawachi, A. L. Gaeta, and M. Lipson, Nature **562**, 401 (2018).
15. A. S. Raja, A. S. Voloshin, H. Guo, S. E. Agafonova, J. Liu, A. S. Gorodnitskiy, M. Karpov, N. G. Pavlov, E. Lucas, R. R. Galiev, A. E. Shitikov, J. D. Jost, M. L. Gorodetsky, and T. J. Kippenberg, Nat. Commun. **10**, 680 (2019).
16. B. Shen, L. Chang, J. Liu, H. Wang, Q.-F. Yang, C. Xiang, R. N. Wang, J. He, T. Liu, W. Xie, J. Guo, D. Kinghorn, L. Wu, Q.-X. Ji, T. J. Kippenberg, K. Vahala, and J. E. Bowers, Nature **582**, 365 (2020).
17. C. Xiang, J. Liu, J. Guo, L. Chang, R. N. Wang, W. Weng, J. Peters, W. Xie, Z. Zhang, J. Riemensberger *et al.*, Science **373**, 99 (2021).
18. L. Chang, S. Liu, and J. E. Bowers, Nat. Photonics **16**, 95 (2022).
19. A. A. Savchenkov, A. B. Matsko, V. S. Ilchenko, and L. Maleki, Opt. Express **15**, 6768 (2007).
20. N. G. Pavlov, G. Lihachev, S. Koptyaev, E. Lucas, M. Karpov, N. M. Kondratiev, I. A. Bilenko, T. J. Kippenberg, and M. L. Gorodetsky, Opt. Lett. **42**, 514 (2017).
21. G. Liu, V. S. Ilchenko, T. Su, Y.-C. Ling, S. Feng, K. Shang, Y. Zhang, W. Liang, A. A. Savchenkov, A. B. Matsko, L. Maleki, and S. J. Ben Yoo, Optica **5**, 219 (2018).
22. N. G. Pavlov, S. Koptyaev, G. V. Lihachev, A. S. Voloshin, A. S. Gorodnitskiy, M. V. Ryabko, S. V. Polonsky, and M. L. Gorodetsky, Nat. Photonics **12**, 694 (2018).
23. E. Lucas, H. Guo, J. D. Jost, M. Karpov, and T. J. Kippenberg, Phys. Rev. A **95**, 043822 (2017).
24. H. Guo, M. Karpov, E. Lucas, A. Kordts, M. H. P. Pfeiffer, V. Brasch, G. Lihachev, V. E. Lobanov, M. L. Gorodetsky, and T. J. Kippenberg, Nat. Phys. **13**, 94 (2017).
25. H. Taheri, A. B. Matsko, L. Maleki, and K. Sacha, Nat. Commun. **13**, 848 (2022).
26. E. Lucas, M. Karpov, H. Guo, M. L. Gorodetsky, and T. J. Kippenberg, Nat. Commun. **8**, 736 (2017).
27. H. Guo, E. Lucas, M. H. P. Pfeiffer, M. Karpov, M. Anderson, J. Liu, M. Geiselmann, J. D. Jost, and T. J. Kippenberg, Phys. Rev. X **7**, 041055 (2017).
28. S.-P. Yu, T. C. Briles, G. T. Moille, X. Lu, S. A. Diddams, K. Srinivasan, and S. B. Papp, Phys. Rev. Appl. **11**, 044017 (2019).
29. Y. Okawachi, B. Y. Kim, Y. Zhao, J. K. Jang, X. Ji, M. Lipson, and A. L. Gaeta, Opt. Lett. **47**, 2234 (2022).
30. X. Liu, C. Sun, B. Xiong, L. Wang, J. Wang, Y. Han, Z. Hao, H. Li, Y. Luo, J. Yan, T. Wei, Y. Zhang, and J. Wang, ACS Photonics **5**, 1943

(2018).
31. H. Weng, J. Liu, A. A. Afridi, J. Li, J. Dai, X. Ma, Y. Zhang, Q. Lu, J. F. Donegan, and W. Guo, Photonics Res. **9**, 1351 (2021).
32. P. Parra-Rivas, D. Gomila, F. Leo, S. Coen, and L. Gelens, Opt. Lett. **39**, 2971 (2014).
33. C. Bao, H. Taheri, L. Zhang, A. Matsko, Y. Yan, P. Liao, L. Maleki, and A. E. Willner, J. Opt. Soc. Am. B **34**, 715 (2017).
34. A. V. Cherenkov, V. E. Lobanov, and M. L. Gorodetsky, Phys. Rev. A **95**, 033810 (2017).
35. S. Fujii and T. Tanabe, Nanophotonics **9**, 1087 (2020).
36. J. Riemensberger, K. Hartinger, T. Herr, V. Brasch, R. Holzwarth, and T. J. Kippenberg, Opt. Express **20**, 27661 (2012).
37. M. Inga, L. Fujii, J. M. C. da Silva Filho, J. H. Quintino Palhares, A. S. Ferlauto, F. C. Marques, T. P. Mayer Alegre, and G. Wiederhecker, APL Photonics **5**, 116107 (2020).